



Low-temperature hydrothermal alteration of intra-caldera tuffs, Miocene Tejada caldera, Gran Canaria, Canary Islands

Eleanor Donoghue^{a,*}, Valentin R. Troll^{a,1}, Chris Harris^b, Aoife O'Halloran^a, Thomas R. Walter^c, Francisco J. Pérez Torrado^d

^a Department of Geology, University of Dublin, Trinity College, Dublin 2, Ireland

^b Department of Geological Sciences, University of Cape Town, Rondebosch 7700, South Africa

^c GFZ Potsdam, Telegrafenberg, 14473 Potsdam, Germany

^d Department of Physics (Geology), University of Las Palmas de Gran Canaria, Canary Islands, Spain

ARTICLE INFO

Article history:

Received 14 September 2007

Accepted 3 May 2008

Available online 20 May 2008

Keywords:

hydrothermal alteration

stable isotopes

Tejada caldera

Gran Canaria

Canary Islands

ABSTRACT

The Miocene Tejada caldera on Gran Canaria erupted ~20 rhyolite–trachyte ignimbrites (Mogán Group 14–13.3 Ma), followed by ~20 phonolitic lava flows and ignimbrites (Fataga Group 13–8.5 Ma). Upper-Mogán tuffs have been severely altered immediately within the caldera margin, whereas extra-caldera Mogán ignimbrites, and overlying Fataga units, are apparently unaltered. The altered intra-caldera samples contain minerals characteristic of secondary fluid–rock interaction (clays, zeolites, adularia), and relics of the primary mineral assemblage identified in unaltered ignimbrites (K-feldspar, plagioclase, pyroxene, amphibole, and groundmass quartz). Major and trace-element data indicate that Si, Na, K, Pb, Sr, and Rb, were strongly mobilized during fluid–rock interaction, whereas Ti, Zr, and Nb behaved in a more refractory manner, experiencing only minor mobilization. The $\delta^{18}\text{O}$ values of the altered intra-caldera tuffs are significantly higher than in unaltered extra-caldera ignimbrites, consistent with an overall low-temperature alteration environment. Unaltered extra-caldera ignimbrites have δD values between -110‰ and -173‰ , which may reflect Rayleigh-type magma degassing and/or post-depositional vapour release. The δD values of the altered intra-caldera tuffs range from -52‰ to -131‰ , with ambient meteoric water at the alteration site estimated at ca. -15‰ . Interaction and equilibration of the intra-caldera tuffs with ambient meteoric water at low temperature can only account for whole-rock δD values of around -45‰ , given that $\Delta\text{D}_{\text{clay-water}}$ is ca. -30‰ at 100 °C, and decreases in magnitude at higher temperatures. All altered tuff samples have δD values that are substantially lower than -45‰ , indicating interaction with a meteoric water source with a δD value more negative than -15‰ , which may have been produced in low-temperature steam fumaroles. Supported by numerical modeling, our Gran Canaria data reflect the near-surface, epithermal part of a larger, fault-controlled hydrothermal system associated with the emplacement of the high-level Fataga magma chamber system. In this near-surface environment, fluid temperatures probably did not exceed 200–250 °C.

© 2008 Elsevier B.V. All rights reserved.

1. Introduction

Caldera margin fault zones are commonly observed to be conduits for fluid flow and hydrothermal activity, and have been shown to affect both the deposition of mineral deposits (Varnes, 1963), and the composition of groundwater contaminated by such mineral deposits (Shevenell and Goff, 1995). The caldera margin rocks on Gran Canaria, Canary Islands, show evidence of severe hydrothermal alteration, and

allow us to study fluid–rock interaction processes in considerable detail. By determining the mineralogy, major- and trace-element concentrations, and whole-rock H- and O-isotope ratios of altered intra-caldera samples, and of equivalent unaltered extra-caldera rocks, we are able to characterise the mineralogical, elemental and isotopic changes brought about by fluid–rock interaction. The stable isotope data yield further constraints on the source of the fluid and its temperature at the time of alteration. The results of this study may help to unravel the complex processes of fluid–rock interaction characteristic of both active and fossil caldera-hosted hydrothermal systems, which are presently inaccessible or poorly exposed.

2. Geological setting

Gran Canaria, one of the central islands of the Canary Archipelago (Fig. 1), is a major oceanic volcano comprising a succession of Miocene

* Corresponding author. Tel.: +353 1 896 1244; fax: +353 1 671 1199.

E-mail addresses: donoghue@tcd.ie (E. Donoghue), Valentin.Troll@geo.uu.se (V.R. Troll), chris.harris@uct.ac.za (C. Harris), ohalloao@tcd.ie (A. O'Halloran), twalter@gfz-potsdam.de (T.R. Walter), fperez@dfis.ulpgc.es (F.J. Pérez Torrado).

¹ Present Address: Department of Earth Sciences, Uppsala University, Villavägen 16, SE-752 36 Uppsala, Sweden.

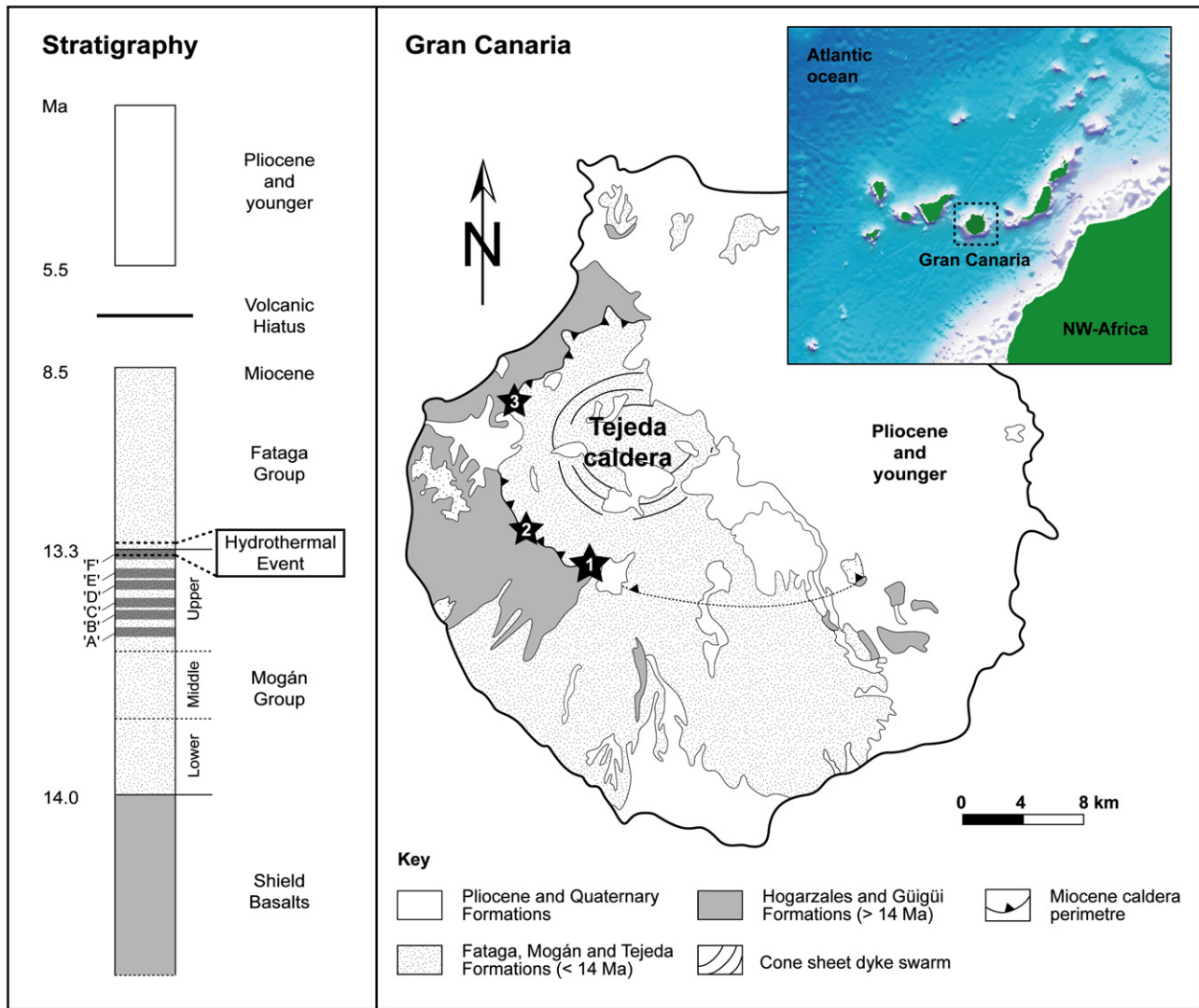


Fig. 1. Simplified geological map of Gran Canaria showing the location of the main sampling area, Fuente de Los Azulejos (1), and two additional localities along the caldera margin where hydrothermally altered tuffs are well-exposed – Tasatico (2), and Fuente Blanca (3). The general sub-aerial stratigraphy of the island is also shown, indicating the approximate stratigraphic levels of upper-Mogán Group ignimbrites 'A', 'B', 'C', 'D', 'E' and 'F' (Schmincke, 1969; Bogaard and Schmincke, 1998).

shield basalts and an overlying series of about 40 felsic ignimbrite sheets and lava flows, which were erupted from the multiply reactivated Tejeda caldera in the centre of the island (Schmincke and Swanson, 1966; Schmincke, 1969, 1982). The felsic stage is subdivided into ~20 trachytic to rhyolitic ignimbrites that erupted between 14 and 13.3 Ma (Mogán Group), and ~20 trachy-phonolitic ignimbrites and lava flows that erupted between 13 and 8.5 Ma (Fataga Group) (Schmincke, 1969, 1982; Bogaard and Schmincke, 1998). Correlation of intra-caldera ignimbrites with the extra-caldera ignimbrite succession suggests subsidence of the caldera basin of at least 1 km (Schmincke and Swanson, 1966; Schmincke 1982; Troll et al., 2002).

A peripheral zone, comprising concentric and radial faults and dykes up to 8 km away from the main caldera margin, is genetically linked to the major caldera fault system (Schmincke, 1982; Troll et al., 2002). Lava flows and ignimbrites locally thicken into the peripheral fault zones, indicating that the faults were active at the time of deposition of these flows (Troll et al., 2002). A well-exposed outer caldera margin on Gran Canaria separates the Miocene shield basalt lavas and overlying felsic extra-caldera ignimbrites from intra-caldera ignimbrites, sediments, and intrusive rocks. The topographic caldera

margin is exposed over km-long stretches in the northwest, west, and southwest of the island. The main study outcrop, Fuente de Los Azulejos, is located on the road between La Aldea and Mogán, in Barranco del Medio (0428353E, 3088999N; Datum UTM; see Fig. 1), and is generally considered the type locality for hydrothermally altered tuffs on Gran Canaria, and the Canary Islands in general (cf. Cabrera Santana et al., 2006). At Fuente de Los Azulejos, the 50°–60° inward dipping caldera margin cuts extra-caldera shield basalts that dip gently towards the sea (Fig. 2A). Tuffs and sediments that fill the caldera pinch out against the steep eroded caldera margin. An up-section decrease in the dip of depositional bedding inside the caldera margin indicates progressive filling of the caldera (Schmincke and Swanson, 1966; Schmincke, 1969). Alteration of the intra-caldera rocks is obvious from their vivid colours (Fig. 2B) and the presence of frequent mineral fills on fractured surfaces (Fig. 3A–H).

The altered intra-caldera tuffs at Fuente de Los Azulejos are late Mogán in age, i.e. they represent a Mogán/Fataga transitional stage (Bogaard and Schmincke, 1998). Their eruptive age is constrained to between the end of upper-Mogán volcanism (13.3 Ma) and the earliest eruption of Fataga units (13.0 Ma) (Bogaard and Schmincke, 1998; Schmincke, 1998; Fig. 1). The altered tuffs are unconformably overlain

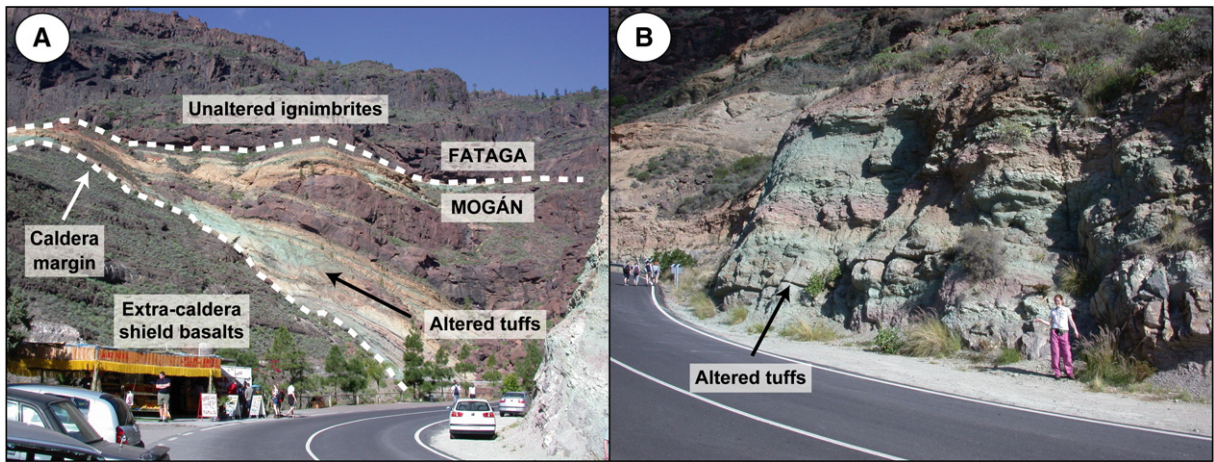


Fig. 2. (A,B): (A) Caldera margin at Fuente de Los Azulejos. Extra-caldera shield basalts (lower left) are unconformably overlain by steeply- to shallowly-dipping intra-caldera tuffs of upper-Mogán age to the top right. This sequence is overlain by apparently unaltered, flat-lying Fataga ignimbrites. (B) Intra-caldera tuffs at Fuente de Los Azulejos displaying vivid green, purple and beige alteration colours (road cutting obliquely opposite coffee shop in A).

by Fataga ignimbrites dated at 12.5 Ma (Bogaard and Schmincke, 1998). These overlying units appear unaltered in the field, suggesting that hydrothermal alteration of the caldera margin tuffs occurred around 13–12.5 Ma. The proposed time range for alteration coincides with the emplacement of an early, high-level Fataga magma chamber system (Schmincke, 1998). Alteration of intra-caldera tuffs is observed all along the exposed caldera margin, with mid- to lower-Mogán lithologies generally displaying a more varied secondary mineralogy relative to upper-Mogán units (Pérez Torrado et al., 2004; Cabrera Santana et al., 2006). The Mogán and Fataga caldera fill was subsequently intruded by syenite stocks and over 500 trachytic to phonolitic cone sheets (12.3–7.3 Ma), representing a late resurgence of the Tejada caldera (Schirmick et al., 1999). Further details on the composition and emplacement mechanisms of the Miocene lavas and ignimbrites can be found in e.g. Schmincke (1969, 1976, 1998), Cousens et al. (1990, 1992), Freundt and Schmincke (1995), Kobberger and Schmincke (1999), Troll and Schmincke (2002), Troll et al. (2003), Hansteen and Troll (2003), and references therein.

3. Petrographic descriptions

Samples were taken from various coloured tuff units exposed along the road section at Fuente de Los Azulejos. Some of the units contain a mixture of alteration colours, in which case we sampled adjacent but differently coloured rocks (Fig. 3A–H; Table 1). Lenses of highly welded glassy tuff, which appeared to have escaped major alteration, were also sampled. In thin section, all samples have a similar primary mineral assemblage, comprising mainly feldspar crystals and crystallites, together with minor pyroxene, amphibole, and groundmass quartz. The samples display a wide range of textures (see Table 1), including brecciated (e.g. HAT 34), glassy (HAT 101), and porphyritic (e.g. HAT 8) varieties. Other features of the suite include the presence of pick-up clasts (HAT 8), mafic xenoliths (e.g. HAT 10), prominent veining, and mineral fills on fracture surfaces (HAT 34).

4. Analytical methods

4.1. X-ray diffraction (XRD)

XRD was carried out on whole-rock samples in the Geochemistry Laboratory in the Geology Department of Trinity College Dublin (TCD), using a Phillips PW1720 X-ray generator and a Phillips PW1050/25 diffractometer. All samples were crushed in a jaw-crusher and powdered using an agate pestle and mortar prior to analysis. The minerals present in each sample were determined by standard XRD meth-

ods using Ni-filtered Cu K α radiation. All measurements were taken from 2°–40° (2 θ) at a step size of 0.02°/sec. X-ray diffractograms were interpreted using “Traces 5.20” software (Hiltonbrooks Ltd, <http://www.xrays.u-net.com/Software.htm>). Identification of minerals was achieved by comparison of peak angles with the Carleton University Department of Geology 2 θ (Cu) table, and the International Centre for Diffractions 1998 powder diffraction database (sets 1–48 and 70–85).

4.2. Scanning electron microscopy (SEM)

SEM was carried out on gold-coated whole-rock chips approximately 1 cm³ in size, using the Hitachi S-4300 high-resolution Scanning Electron Microscope (SEM) housed in the Centre for Microscopy and Analysis at TCD (see <http://www.tcd.ie/CMA/s4300.htm> for a detailed description of the equipment and analytical procedure). The samples were taken predominantly from the type locality, Fuente de Los Azulejos. Additional SEM investigations have been carried out on a small number of samples from Fuente Blanca and Tasartico (see Fig. 1 for locations), where hydrothermally altered tuffs are also exposed. These additional samples were analysed using the JEOL-JSM 840 SEM housed at the University of Alicante, Spain. In both cases, the SEM was run in secondary electron mode.

4.3. X-ray fluorescence (XRF)

Powdered whole-rock samples were dried at 110 °C prior to analysis. Major and trace-element concentrations were determined on fused beads using an automated Philips PW1480 spectrometer at GEOMAR Research Centre, Kiel, Germany. All analyses were performed with an Rh tube. A full description of the methods employed, and the associated errors, are given in Abratis et al. (2002), and Troll and Schmincke (2002).

4.4. Stable isotopes

For the altered tuff samples with prefix “HAT”, O- and H₂O-extractions were carried out in Université Jean Monnet (UJM), St-Etienne, France. For altered samples with prefix “GC”, and the unaltered extra-caldera ignimbrites, O- and H₂O-extractions were carried out in the University of Cape Town (UCT), South Africa. The D/H and ¹⁸O/¹⁶O ratios were determined with a VG Isoprime mass spectrometer in UJM, and with a Finnigan MAT252 mass spectrometer in UCT.

Whole-rock samples were prepared for D/H determination in both laboratories using the method of Vennemann and O’Neil (1993). All samples were degassed on a conventional silicate vacuum line at

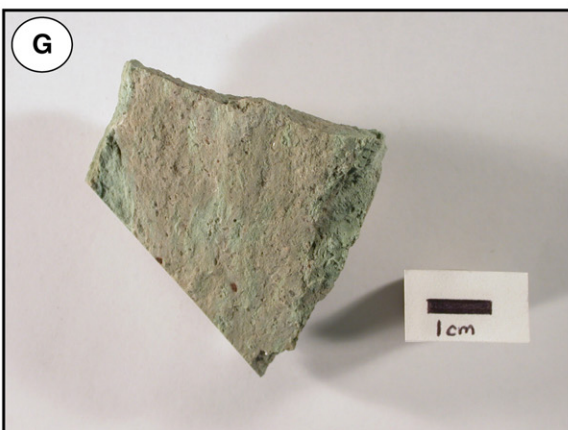
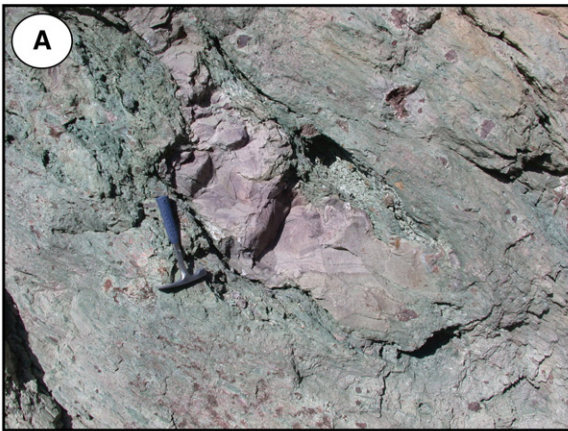


Table 1
Name, colour, and petrographic features of the hydrothermally altered tuffs (HAT) from Fuente de Los Azulejos, Gran Canaria

Sample name	Sample type	Colour	Notable petrographic features
HAT 3	Tuff matrix	Green	Fine-grained, pervasively altered matrix with fluidal texture; fibrous texture in places; fragmented and partially replaced plagioclase phenocrysts;
HAT 5	Fiammé (in HAT 6)	Purple	40% opaques; strongly silicified groundmass; minor quartz veining;
HAT 6	Tuff matrix	Green	Fragmented and partially replaced K-spar + plagioclase phenocrysts; plagioclase-rich mafic xenoliths with quartz rims; pervasively altered, fine-grained groundmass with fluidal texture;
HAT 7	Tuff matrix	Orange/yellow	Fragmented plagioclase phenocrysts with crystal-boundary alteration; pervasively altered groundmass with fluidal texture;
HAT 8	Tuff matrix	Orange	Brecciated texture; contains rip-up clasts of green altered tuff; primary relics in clasts and host tuff; K-spar + plagioclase phenocrysts partially replaced; pervasively altered mafic xenoliths;
HAT 9	Tuff matrix	Green/red	Green matrix dominates, red matrix patchy; gradation between green and red matrix; fine-grained, strongly altered groundmass; fragmented plagioclase phenocrysts partially replaced along crystal boundaries and fractures; altered mafic xenoliths;
HAT 10	Tuff matrix	Green	Partially replaced mafic xenoliths, K-spar and plagioclase phenocrysts; pervasively altered matrix with fluidal texture;
HAT 11	Tuff matrix	Green	Prominent veining in groundmass; partially replaced fragmented plagioclase phenocrysts; mafic xenoliths rare/absent;
HAT 5.5	Tuff matrix	Grey/green	Partially replaced mafic xenoliths, K-spar and plagioclase phenocrysts; fine-grained, pervasively altered matrix with fluidal texture;
HAT 33	Tuff matrix	Green	Partially replaced plagioclase phenocrysts; fine-grained, pervasively altered groundmass with fluidal texture;
HAT 34	Tuff matrix	Pink	Plagioclase phenocrysts and plagioclase-rich mafic xenoliths with grain boundary alteration; brecciated, fluidal texture in groundmass; fibrous texture in places;
HAT 101	Tuff matrix	Dark green	Partially replaced mafic xenoliths; plagioclase and K-spar phenocrysts with alteration along crystal boundaries; glassy groundmass with perlitic cracks and fractures; clay alteration along fractures;
HAT 102	Tuff matrix	Grey/green	Opaque-rich groundmass with prominent veining; plagioclase phenocrysts with crystal-boundary alteration; partially replaced plagioclase-rich mafic xenoliths.

200 °C prior to pyrolysis. For altered samples, water was liberated from ~50 mg of whole-rock powder, and ~100 mg of 'Indiana' Zn was used to reduce the liberated water to H₂. For unaltered samples, 200 mg of sample powder and 200–300 mg of Zn were used to ensure enough H₂O was liberated and reduced to H₂ for analysis. Water was produced from ~50 mg of an internal biotite standard (CGBi, δD = -59‰) and analysed in duplicate with each batch of samples. For D/H determination, an internal water standard (CTMP, δD = -9‰) was used to calibrate the raw data to the SMOW scale, and the data were normalized so that V-SLAP gave a value of -428‰ on the SMOW scale, as recommended by Coplen (1995). Water concentrations of whole rocks were determined from the voltage measured on the mass 2 collector of the mass spectrometer using identical sample inlet volume (Vennemann and O'Neil, 1993).

For O-isotopes, whole-rock samples were dried in an oven at 50 °C, and degassed under vacuum on a conventional silicate line at 200 °C for 2 h. Silicate minerals were reacted with BrF₅ (UJM) or ClF₃ (UCT; cf. Borthwick and Harmon, 1982) in the silicate line for 3 h at 550 °C, and the liberated O₂ was converted to CO₂ using a hot platinized carbon rod. Further details on the methods employed for O-extraction from silicate minerals at UCT can be found in Vennemann and Smith (1990) and Harris and Erlank (1992). The extraction procedure at UJM is described by Gerbe and Thouret (2004). In UJM, the δ¹⁸O value obtained for an internal standard (Murchison Line Quartz, MQ; δ¹⁸O = 10.1‰) was used to normalize the raw δ¹⁸O data to the SMOW scale. In UCT, the internal quartz standard NBS-28 (δ¹⁸O = 9.64‰) was used for normalization to the SMOW scale (cf. Coplen et al., 1983). The normalized and un-normalized values differ by <0.4‰. The analytical error for δ¹⁸O is about ±0.1‰ (1σ) for all samples. For δD and H₂O⁺, the analytical errors are typically of the order of ±2‰ (1σ) and 0.10 wt.%, respectively, but the error on δD increases as the amount of water extracted decreases. The measured blank associated with the H₂O-extraction method is extremely small, but highly negative (there is insufficient gas to measure the δD accurately). It is, therefore, possible that the very negative δD values in samples with low water content represent a proportionally higher component from the blank. However, duplicate analyses on three ignimbrite 'A' samples (see Table 4), and subsequent work on similar samples, has shown that the very low δD

values are reproducible. This suggests that contamination by D-depleted blank water in the silicate line during H₂O-extraction is unlikely to be significant, and is not the cause of the low δD values. All data are reported in the familiar δ notation where δ = 1000 * ((R_{sample} - R_{standard}) / R_{standard}) and R = ¹⁸O/¹⁶O or D/H.

5. Results

5.1. Mineralogy

The results of the XRD analyses are summarised in Table 2. Unaltered extra-caldera ignimbrites contain mainly K-feldspar and plagioclase, and minor pyroxene, amphibole, and groundmass quartz (cf. Schmincke, 1969, 1982; Sumita and Schmincke, 1998). The altered intra-caldera tuffs contain relics of this primary mineral assemblage, as well as a distinct secondary mineralogy comprising mainly clays, zeolites, analcite, and alteration feldspar (e.g. adularia), indicative of significant fluid-rock interaction (cf. Deer et al., 1966; García del Cura et al., 1999; Cabrera Santana et al., 2006).

The results of SEM (Fig. 4A–H) place further constraints on the composition and morphology of the alteration mineral assemblage. All samples have a high proportion of clay minerals (Fig. 4A, B), which typically form globular (e.g. smectite) and fibrous/whispy aggregates (e.g. illite). The altered tuffs also contain a diverse range of zeolites (Fig. 4C–F), including clinoptilolite (tabular), analcite (polyhedral), mordenite and erionite (fibrous). HAT 101, the highly welded glassy tuff, displays clay alteration along fractures and perlitic cracks (Fig. 4G), indicating that this sample has in fact undergone some water-rock interaction, despite its apparently fresh appearance in hand sample. Relics of the primary mineralogy, such as disarticulated and partially replaced phenocrysts (e.g. pyroxene in HAT 102; Fig. 4H), can also be identified in some samples.

5.2. Major and trace elements

The major and trace-element concentrations of the altered tuffs from Fuente de Los Azulejos are given in Table 3. Harker plots for selected elements are shown in Figs. 6 and 7, and include data for

Fig. 3. (A–H): (A) Fiammé (HAT 5) showing different colouration to its host ignimbrite (HAT 6). (B) Mix of colours within an ignimbrite unit (HAT 9). (C) HAT 8 showing orange alteration colours. (D) HAT 6 showing green alteration colours. (E) Dark green, highly welded glassy tuff (HAT 101). (F) Brecciated HAT 34 showing pink/orange alteration colours. Note the presence of mineral fills on fracture surfaces, and conspicuous veining in the matrix. (G) HAT 102 showing grey/green alteration colours. (H) HAT 5.5 showing grey/green alteration colours and dark brown mineral fills.

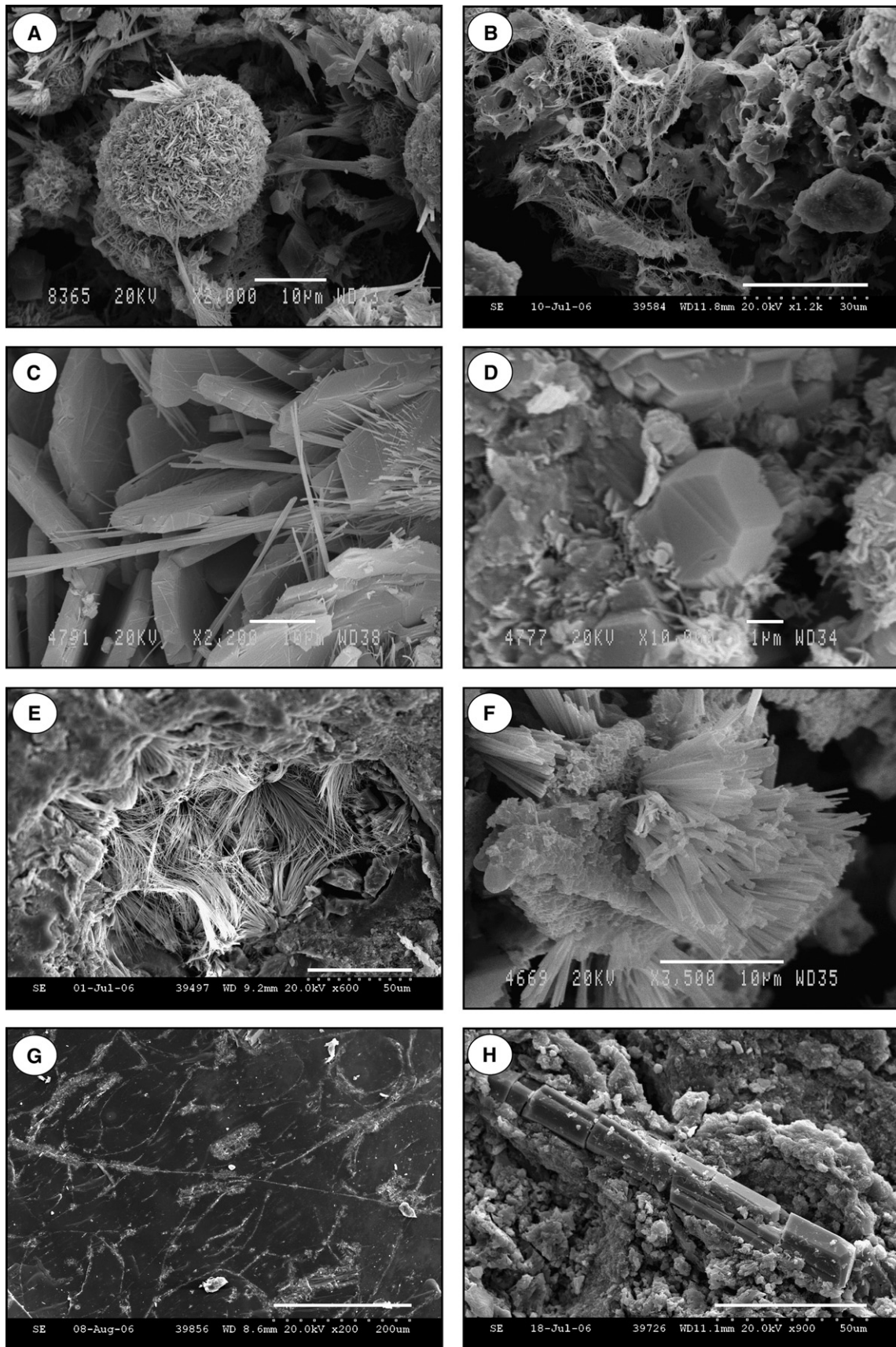


Fig. 4. (A–H): Secondary electron SEM images of a selection of altered tuff samples taken from the type locality, Fuente de Los Azulejos (B, E, G, and H), and two additional localities in western Gran Canaria – Tasartico (A), and Fuente Blanca (C, D, and F) (cf. [Cabrera Santana et al., 2006](#)). (A) Clay mineral (smectite) forming globular aggregates. (B) Clay mineral (illite) forming whispy aggregates. (C) Tabular zeolite crystals (clinoptilolite). (D) Polyhedral zeolite crystals (analcite). (E) Fibrous zeolite crystals (mordenite). (F) Radiating zeolite crystals (erionite). (G) Clay alteration along fractures and perlitic cracks in a sample of highly welded glassy tuff. (H) Relict primary pyroxene phenocryst showing partial alteration by clay minerals, mainly along fractured surfaces. Image number, accelerating voltage (in KV), magnification, scale (in μm), and working distance (WD) are given at the bottom of each image.

Table 2

Distribution of minerals between altered intra-caldera samples and unaltered extra-caldera ignimbrites 'A', 'D', 'E', and 'F' from XRD results

Samples	Primary minerals ^a					Secondary minerals ^b					
	K-spar	plag	pyx	amph	qtz (g/v) ^c	mont/chl-mont	qtz (h) ^c	mord	anal	adul	ill
Altered	HAT 5	X		X		X	X	X			
	HAT 6	X	X			X	X	X	X		
	HAT 7	X	X			X	X	X		X	X
	HAT 8	X		X		X	X	X	X		
	HAT 9	X	X	X		X	X		X		X
	HAT 10	X		X		X	X	X	X		X
	HAT 11	X	X	X		X	X	X	X	X	X
	HAT 5.5	X				X	X		X		
	HAT 33		X			X	X				
	HAT 34	X	X			X	X	X			
	HAT 101	X	X			X	X	X		X	
HAT 102	X	X			X	X	X	X	X	X	
Unaltered	A3F3	X	X	X							
	A4F6	X	X	X		X					
	DTF2	X	X		X	X					
	ECF	X	X		X	X					
	FTF8	X		X	X						

^a K-spar = K-feldspar, plag = plagioclase, pyx = pyroxene, amph = amphibole, qtz (g/v) = groundmass/vapour-phase quartz.^b mont = montmorillonite, chl-mont = chlorite-montmorillonite, qtz (h) = hydrothermal quartz, mord = mordenite, anal = analcite, adul = adularia, ill = illite.^c Distinction between primary and secondary quartz based on thin section observations.**Table 3**

Major and trace-element concentrations of the hydrothermally altered tuffs (HAT) from Fuente de Los Azulejos, Gran Canaria

	HAT 3	HAT 5	HAT 6	HAT 7	HAT 8	HAT 9	HAT 10	HAT 11	HAT 5.5	HAT 33	HAT 34	HAT 101	HAT 102
<i>wt.%</i>													
SiO ₂	65.82	77.59	58.74	68.21	66.93	66.93	69.56	63.06	65.84	76.81	71.15	64.9	61.89
TiO ₂	0.67	0.37	1.04	0.68	0.83	0.71	0.73	0.78	0.8	0.56	0.61	0.71	0.81
Al ₂ O ₃	12.44	7.94	15.51	11.86	12.62	14.19	11.28	13.83	14.86	8.77	10.22	12.34	14.63
Fe ₂ O ₃	4.91	4.43	6.39	4.63	5.18	4.27	4.9	5.65	4.34	3.88	4.17	5.46	5.47
MnO	0.17	0.12	0.28	0.18	0.27	0.11	0.31	0.19	0.47	0.05	0.23	0.28	0.53
MgO	0.71	0.41	0.93	0.59	1	0.86	0.95	0.84	0.69	0.54	0.42	0.53	0.85
CaO	0.98	0.57	0.98	0.84	0.8	0.32	0.77	0.86	0.44	0.66	1.04	0.49	0.74
Na ₂ O	2.12	2.1	5.61	3.42	2.84	3.85	2.3	3.74	3.69	1.05	2.83	5.29	3.89
K ₂ O	5.28	4.43	4.14	4.06	4.77	4.2	5.14	4.72	4.25	3.39	3.06	3.05	4.74
P ₂ O ₅	0.07	0.06	0.14	0.08	0.09	0.09	0.08	0.1	0.1	0.05	0.06	0.07	0.1
Sum	93.17	98.02	93.76	94.55	95.33	95.53	96.02	93.77	95.48	95.76	93.79	93.12	93.65
LOI	6.20	2.24	5.95	5.36	4.26	4.18	3.91	6.08	3.99	2.97	5.44	5.90	5.54
<i>ppm</i>													
Co	5	5	<4	6	10	<4	11	<4	10	5	7	<4	7
Ni	2	2	8	2	2	2	2	2	20	15	10	5	9
V	12	34	90	15	29	16	24	23	43	33	12	37	43
Zn	346	96	390	257	351	222	287	341	249	202	238	296	328
Ce	477	205	437	334	326	319	291	386	314	318	305	391	444
La	164	49	177	93	143	99	121	154	84	44	52	93	180
Nb	248	270	327	286	282	249	246	303	270	277	285	323	348
Ga	38	20	45	31	36	37	33	42	36	24	24	40	40
Pb	4	21	24	18	11	14	23	19	19	12	26	15	29
Rb	154	72	172	125	163	147	162	174	110	124	95	151	128
Ba	102	27	90	39	49	150	56	201	259	20	72	134	518
Sr	101	5	46	19	31	15	18	35	33	9	31	16	27
Th	35	16	32	24	25	20	28	24	18	32	24	31	40
Y	115	89	152	107	127	99	125	138	93	123	86	124	143
Zr	2096	1675	1979	1779	1784	1646	1888	1776	1492	1835	1311	2004	2088

unaltered extra-caldera ignimbrites 'A' (Troll and Schmincke, 2002) and 'D' (Kobberger and Schmincke, 1999) for comparison. All plotted data are normalized to 100% on a volatile-free basis. The altered tuff samples plot in the trachyte to rhyolite fields on a Total Alkali versus Silica (TAS) diagram (Le Maitre et al., 1989; Fig. 5), and define an overall trend of decreasing Na₂O+K₂O with increasing SiO₂. The altered tuffs have a much wider range of SiO₂ concentrations (62.7–80.2 wt.%)² than the unaltered extra-caldera ignimbrites 'A' (66.7–

70.8 wt.%) and 'D' (65.2–69.0 wt.%), and have distinctly lower total alkali concentrations, reflecting substantial Na and/or K loss. On plots of immobile elements (e.g. TiO₂) versus SiO₂ (Fig. 6A), the unaltered extra-caldera ignimbrites show well-correlated magmatic differentiation trends (Kobberger and Schmincke, 1999; Troll and Schmincke, 2002; Troll et al., 2003). The altered tuffs also define a relatively well-correlated linear trend, but over a much wider range of SiO₂ concentrations than the unaltered ignimbrites. On plots of TiO₂ versus Nb (Fig. 7A), and Zr versus Nb (Fig. 7B), the altered tuffs show rather scattered patterns relative to unaltered ignimbrites 'A' and 'D', both of which define well-correlated magmatic differentiation

² All quoted SiO₂ data are normalized to 100 % on a volatile-free basis.

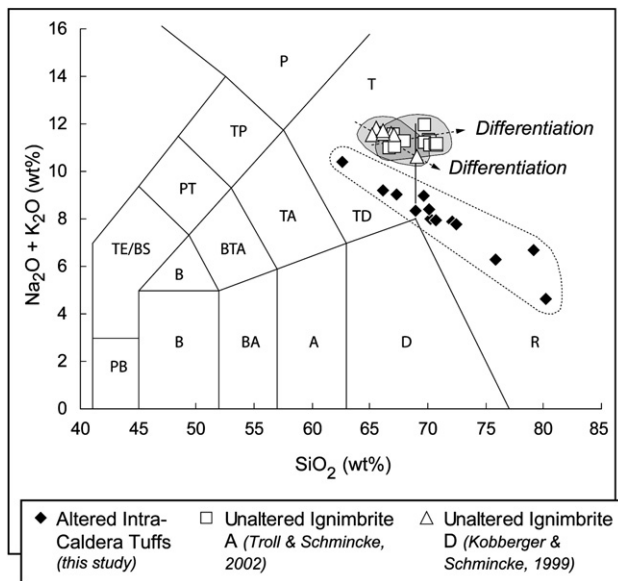


Fig. 5. Total Alkali versus Silica (TAS) diagram (Le Maitre et al., 1989) showing the classification of the altered tuff samples. Also plotted for comparison are unaltered extra-caldera upper-Mogán ignimbrites 'A' (data from Troll and Schmincke, 2002) and 'D' (data from Kobberger and Schmincke, 1999). Abbreviations: PB = micro-basalt, B = basalt, BA = basaltic-andesite, A = andesite, D = dacite, R = rhyolite, BTA = basaltic trachy-andesite, TA = trachy-andesite, TD = trachy-dacite, T = trachyte, TE = tephrite, BS = basanite, PT = phono-tephrite, TP = tephri-phonolite, P = phonolite. All data points lie in the trachyte to rhyolite fields. However, note the wide range of SiO_2 wt.% concentrations and lower total alkali ($\text{Na}_2\text{O} + \text{K}_2\text{O}$ wt.%) concentrations of the altered samples relative to the unaltered ignimbrites (see Section 6.2 for details).

trends. In addition, Zr and Nb concentrations in the altered tuffs plot at the higher end of the range of values recorded in the unaltered extra-caldera rocks. On plots of strongly fluid-mobile elements (e.g. K, Pb, Sr, Rb) against SiO_2 (Fig. 6B–F) and Nb (Fig. 7C–G), the altered tuffs show highly scattered patterns relative to the unaltered ignimbrites.

5.3. Stable isotopes

The O- and H-isotope compositions and water concentrations of the altered intra-caldera tuffs and unaltered extra-caldera ignimbrites are given in Table 4. The δD values of the altered tuffs lie between -52‰ and -131‰ ($n=21$), while unaltered tuffs have δD values between -110‰ and -173‰ ($n=9$) (Fig. 8A, B). Water concentrations up to ~ 4 wt.% are found in the altered caldera margin tuffs, compared to ≤ 0.2 wt.% H_2O in unaltered extra-caldera samples (Fig. 8B). The altered caldera margin tuffs have $\delta^{18}\text{O}$ values of 12–18‰ ($n=21$), which are considerably higher than the $\delta^{18}\text{O}$ values obtained for the unaltered extra-caldera ignimbrites (6.5–7.1‰, $n=6$) (Fig. 9), and those reported for the Mogán Group in the literature (Cousens et al., 1992; Troll and Schmincke, 2002; Hansteen and Troll, 2003). The apparently unaltered, highly welded glassy tuff from the intra-caldera

section (HAT 101; Fig. 3E) plots well within the δD – $\delta^{18}\text{O}$ field defined by the altered tuffs (Table 4; Fig. 9), and has a relatively high water concentration of 2.3 wt.%. The isotopic results for HAT 101 confirm our earlier deductions from mineralogy (see Section 5.1), that this

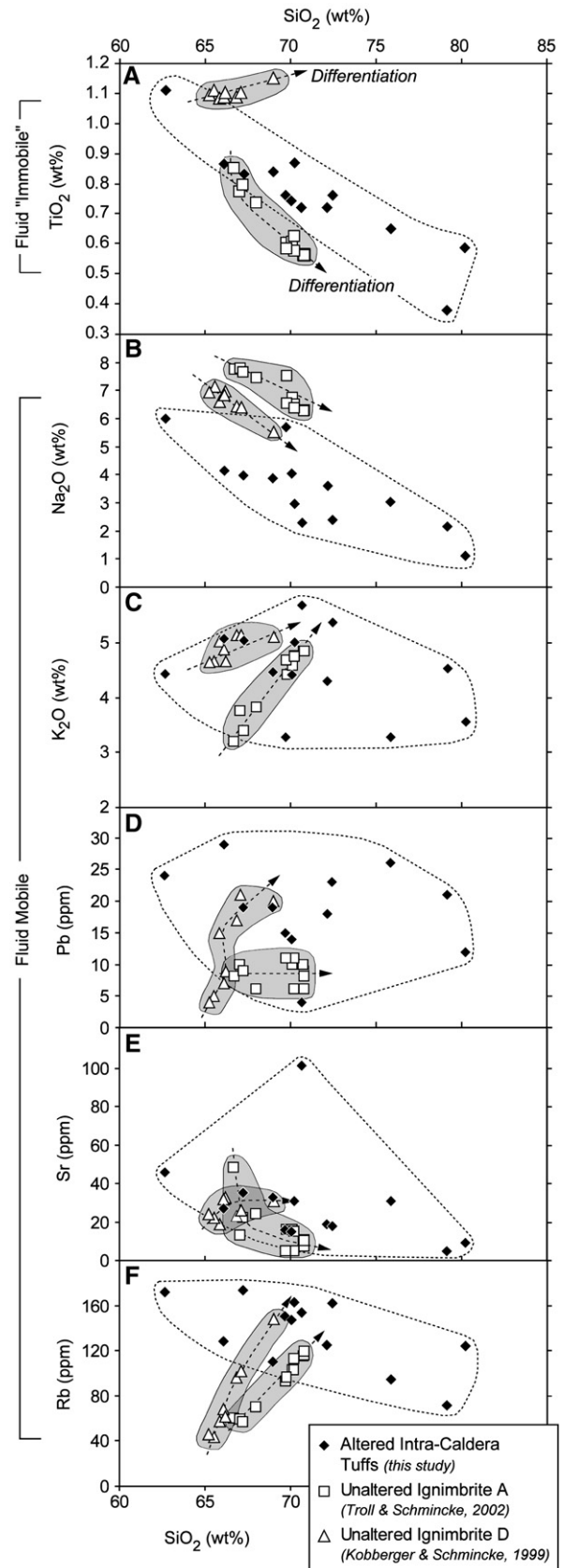
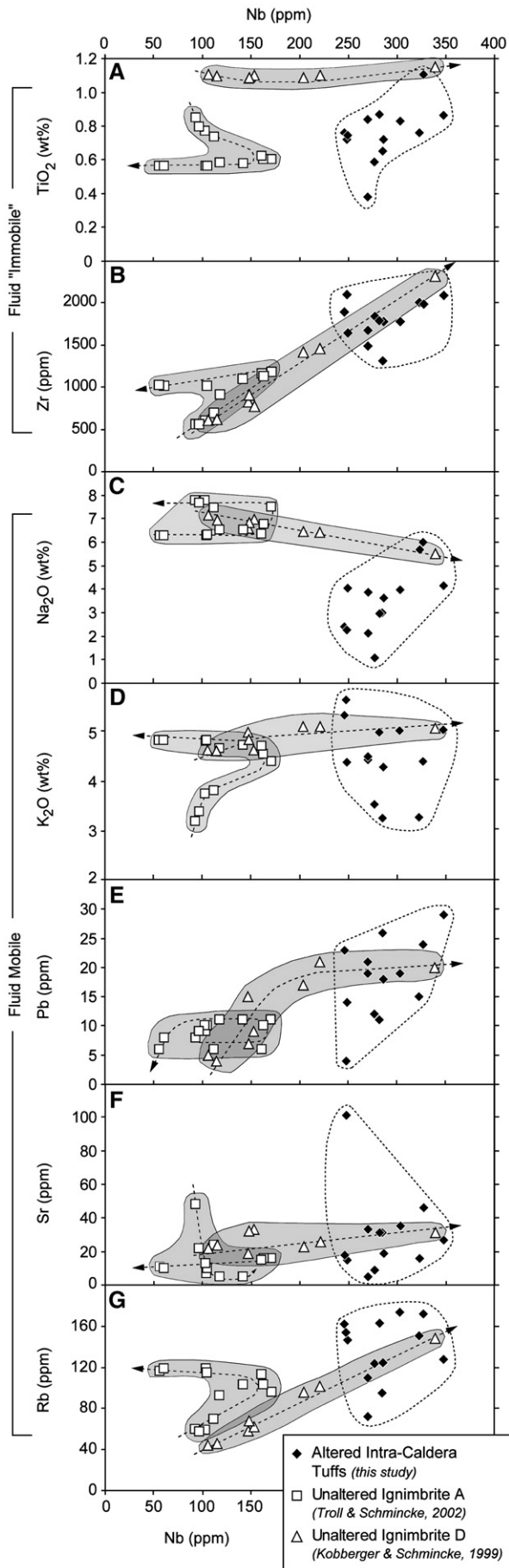


Fig. 6. (A–F): Plots of fluid-immobile (TiO_2) and fluid-mobile (K_2O , Na_2O , Pb, Sr, Rb) elements versus SiO_2 for the hydrothermally altered tuff samples, and unaltered extra-caldera ignimbrites 'A' (Troll and Schmincke, 2002) and 'D' (Kobberger and Schmincke, 1999). The unaltered ignimbrites define well-correlated linear or curvilinear trends (dashed arrows) on all plots, representing the effects of original magmatic differentiation, mainly by fractional crystallisation. The altered tuffs show a relatively good TiO_2 – SiO_2 correlation (A), but the data points define a much larger field than the unaltered ignimbrites, most likely reflecting strong Si (and perhaps some Ti) mobilization during low-temperature fluid–rock interaction (see Section 6.2 for details). The data points for the altered tuffs are highly scattered on all fluid-mobile element plots (B–F), indicating either loss or gain of these elements due to hydrothermal alteration of the sample suite.



apparently fresh sample has actually undergone significant hydrous alteration.

6. Discussion

6.1. Mineralogy

The altered intra-caldera tuffs consist predominantly of clay minerals, zeolites and adularia, as well as relics of the primary mineralogy (K-feldspar, plagioclase, pyroxene, amphibole, and groundmass quartz; cf. Sumita and Schmincke, 1998). The presence of clay minerals (e.g. illite) is a characteristic feature of hydrous alteration of volcanic glass, and of ferromagnesian sheet silicates such as phlogopite (Deer et al., 1966), a common phase in the Mogán ignimbrites (Schmincke, 1982, 1998; Sumita and Schmincke, 1998). Zeolites (e.g. clinoptilolite, mordenite, erionite), and the hydrated aluminosilicate analcite, occur abundantly in the altered tuffs (cf. García del Cura et al., 1999; Cabrera Santana et al., 2006), and are strong indicators of low-temperature (and therefore shallow) alteration (Deer et al., 1966). Traces of wairakite, a calcium end-member of analcite first defined from Wairaki hydrothermal field, New Zealand (cf. Schröcke and Weiner, 1981), also occur in the altered tuffs. Adularia, found in a number of samples, is a low-temperature potassium feldspar that commonly forms in alteration cracks and veins (Deer et al., 1966). The observed secondary mineral assemblage, therefore, reflects a classic low-temperature (≤ 250 °C) alteration environment, indicative of a shallow, epithermal system.

6.2. Element mobility

The altered caldera margin tuffs show a wide range of SiO_2 wt.% concentrations relative to unaltered ignimbrites 'A' and 'D' (Figs. 5 and 6A–F), suggesting that Si has been either enriched or depleted in the various samples of the suite during low-temperature fluid–rock interaction. Further evidence for Si mobility can be seen in thin sections of the altered tuffs, some of which display partially silicified matrices and quartz-lined fractures (see Table 1). Almost all of the altered tuff samples have lower Na_2O wt.% concentrations than the unaltered ignimbrites, indicating that Na has been mobilized and leached from the tuffs by the hydrothermal fluid (Fig. 6B). Other strongly fluid-mobile elements (e.g. K, Sr, Pb, Rb) produce rather scattered patterns when plotted against SiO_2 (Fig. 6C–F) and immobile incompatible elements such as Nb (Fig. 7D–G). This is in stark contrast to unaltered ignimbrites 'A' and 'D', which both show well-correlated original igneous evolutionary trends on all plots (Kobberger and Schmincke, 1999; Troll and Schmincke, 2002; Troll et al., 2003). The scattered patterns for the altered tuffs suggest that significant secondary addition or loss of K, Sr, Pb, and Rb has occurred during low-temperature water–rock interaction, causing any original igneous trends to be completely obliterated.

Further support for low-temperature Sr and Pb mobility during alteration is provided by radiogenic isotope data. Initial Sr-isotope ratios of up to 0.704 are seen in the unaltered Mogán and Fataga

Fig. 7. (A–G): Plots of fluid – 'immobile' (TiO_2 and Zr) and fluid-mobile (K_2O , Na_2O , Pb, Sr, Rb) elements versus Nb for the hydrothermally altered tuff samples, and unaltered extra-caldera ignimbrites 'A' (Troll and Schmincke, 2002) and 'D' (Kobberger and Schmincke, 1999). Ignimbrites 'A' and 'D' define original magmatic trends (dashed arrows) due to fractional crystallisation of feldspar, pyroxene, amphibole, and (for ignimbrite 'A') late-stage crystallisation of the REE mineral chevkinite, which preferentially fractionates Nb over Zr into the mineral lattice (Troll et al., 2003). The altered tuffs are relatively enriched in Zr and Nb, indicating that these elements were dominantly refractory during fluid–rock interaction. However, note the relatively scattered patterns for the altered tuffs in A and B, perhaps reflecting minor mobilization of Ti, Zr, and Nb (see Section 6.2 for details). On all fluid-mobile element plots (C–G), the data points for the altered tuffs are highly scattered, reflecting strong mobilization of these elements during secondary fluid–rock interaction.

ignimbrites (Cousens et al., 1990). Sample HAT 3, however, shows an initial $^{87}\text{Sr}/^{86}\text{Sr}$ ratio of 0.708364 (9) (Troll, 2001), suggesting that fluid–rock interaction may have raised Sr-isotope ratios significantly. This shift is also reflected in the more radiogenic $^{206}\text{Pb}/^{204}\text{Pb}$ values in the altered tuff sample relative to unaltered Mogán rocks (Troll, 2001). This increase in radiogenic isotope ratios is consistent with strong Sr and Pb mobility in a system where hydrothermal fluids are the major transporting agents.

On plots of immobile elements (e.g. TiO_2) versus SiO_2 (Fig. 6A), the altered tuffs define a relatively well-correlated linear trend, which may crudely reflect magmatic differentiation processes. However, given the relatively wide range of SiO_2 wt.% concentrations in the altered tuffs, it is likely that Si has been mobilized during secondary fluid–rock interaction, and such a correlation is therefore no longer a reliable index of magmatic evolution. Furthermore, the poor correlation between Ti and Nb in the altered tuffs (Fig. 7A) suggests that some low-temperature mobilization of at least one of these elements has also occurred, modifying any original igneous trends. Similarly, on a plot of Zr versus Nb (Fig. 7B), the altered tuffs define a relatively scattered pattern, whereas unaltered ignimbrites 'A' and 'D' show well-correlated igneous evolutionary trends, partly reflecting fractionation of Rare Earth Element (REE) minerals (cf. Troll et al., 2003). The poor correlation between Zr and Nb in the altered tuffs suggests that these elements have been mobilized to some extent. This is consistent with the findings of Hill et al. (2001), who have shown that many elements traditionally regarded as 'fluid-immobile' (e.g. Ti, Nb, and Zr) can in fact be variably enriched or depleted during low-temperature processes, such as weathering and hydrothermal alteration. However, the crude TiO_2 – SiO_2 correlation, and the overall enriched Zr and Nb concentrations in the altered tuffs relative to the unaltered rocks,

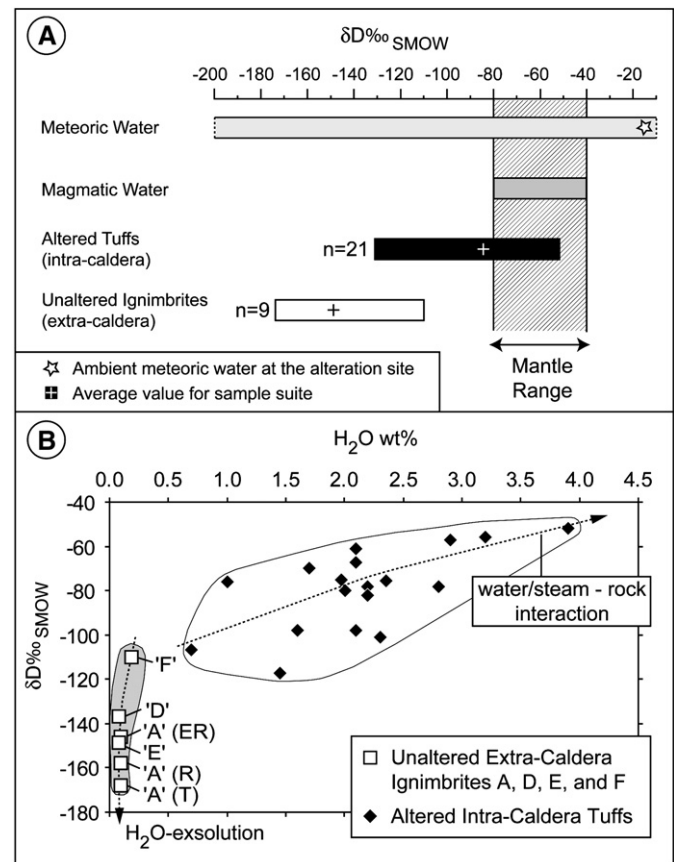


Fig. 8. (A,B): (A) Bar chart showing the range of whole-rock δD values obtained for the altered intra-caldera tuffs, and unaltered extra-caldera ignimbrites. The average δD value is shown for each sample suite. Also shown is the estimated δD of ambient meteoric water at the alteration site ($\delta\text{D} = -15\text{‰}$), and the δD ranges typical of magmatic and meteoric waters, and mantle rocks (Taylor, 1986 and references therein). (B) Plot of whole-rock δD versus H_2O wt.% for the altered intra-caldera tuffs, and unaltered extra-caldera ignimbrites 'A', 'D', 'E' and 'F'. Average values are plotted for samples analysed in duplicate. The altered tuffs show elevated water concentrations and δD compositions relative to the unaltered ignimbrites, indicative of interaction with a local meteoric water source. The very low hydrogen isotope ratios of the unaltered ignimbrites reflect loss of water during degassing resulting in extreme deuterium depletion in this sample suite. Note that compositionally zoned ignimbrite 'A' (cf. Troll and Schmincke, 2002) is generally more depleted in deuterium than ignimbrite 'F', and shows a systematic decrease in δD values from its base (evolved rhyolite – ER), to its centre (rhyolite – R), to its top (trachyte – T). See Section 6.3 for details.

indicates that Ti, Zr and Nb were largely refractory during water–rock interaction, and were preferentially retained in minor phenocryst (e.g. titanite, zircon and chevkinite; cf. Troll et al., 2003) and groundmass phases (e.g. aegirine and arfvedsonite).

6.3. Stable isotopes

The whole-rock δD values of unaltered ignimbrites range from -110‰ to -173‰ , and are accompanied by relatively low H_2O concentrations (≤ 0.2 wt.%) (Fig. 8A, B). Such low δD and H_2O wt.% values are characteristic of Rayleigh-type H_2O -vapour exsolution from the crystallising magma prior to eruption, causing the residual melt, and any late-stage hydrous phases crystallising from this melt (e.g. amphibole), to become progressively depleted in D and H_2O (cf. Nabelek et al., 1983; Taylor et al., 1983; Taylor, 1986). Degassing during eruption, and/or during post-depositional vapour release may have caused further depletion in D and H_2O in the unaltered ignimbrites. It is also worth noting that there is an apparent correlation between δD and the relative stratigraphic positions of the extra-caldera ignimbrites, i.e.

Table 4

Stable isotope ($\delta^{18}\text{O}\text{‰}$ and $\delta\text{D}\text{‰}$) and H_2O wt.% values for the hydrothermally altered tuff samples from Fuente de Los Azulejos, and for unaltered samples of extra-caldera ignimbrites 'A', 'D', 'E', and 'F'

Sample type	Sample name	$\delta^{18}\text{O}\text{‰}$	$\delta\text{D}\text{‰}$	H_2O wt.%	
Altered tuffs (intra-caldera)	HAT 3	16.2	-78	2.8	
	HAT 5	14.9	-76	1.0	
	HAT 6	14.6	-52	3.9	
	HAT 7	18.4	-67	2.1	
	HAT 8	13.5	-57	2.9	
	HAT 9	13.9	-56	3.2	
	HAT 10	13.3	-78	2.2	
	HAT 11	17.3	-61	2.1	
	HAT 5.5	12.6	-75	2.4	
	HAT 33 ^a	13.4	-103	1.5	
		14.0	-131	1.4	
	HAT 34	16.5	-75	2.0	
	HAT 101 ^a	16.8	-97	2.5	
		16.2	-105	2.2	
	HAT 102	14.8	-80	2.0	
	GC29	12.0	-70	1.7	
	GC48 ^a	11.9	-92	0.8	
		15.2	-121	0.5	
		GC91	16.3	-98	2.1
		GC78	12.4	-82	2.2
	GC97	12.3	-98	1.6	
Unaltered ignimbrites (extra-caldera)	A-III-F8-Bto (T) ^a	6.7	-173	0.1	
			-162	0.1	
	A-III-F12-Bto (R) ^a	6.5	-169	0.1	
			-146	0.1	
	A-F1-BTTS (ER) ^a	7.0	-149	0.1	
			-142	0.1	
	D-III-F1-BMA	7.2	-137	0.1	
	E-F1-BTo	6.7	-149	0.1	
	FI-F2-BTo	7.1	-110	0.2	

T = trachyte, R = rhyolite, ER = evolved rhyolite (cf. Troll and Schmincke, 2002).

^a Sample analysed in duplicate for $\delta^{18}\text{O}$ and/or δD .

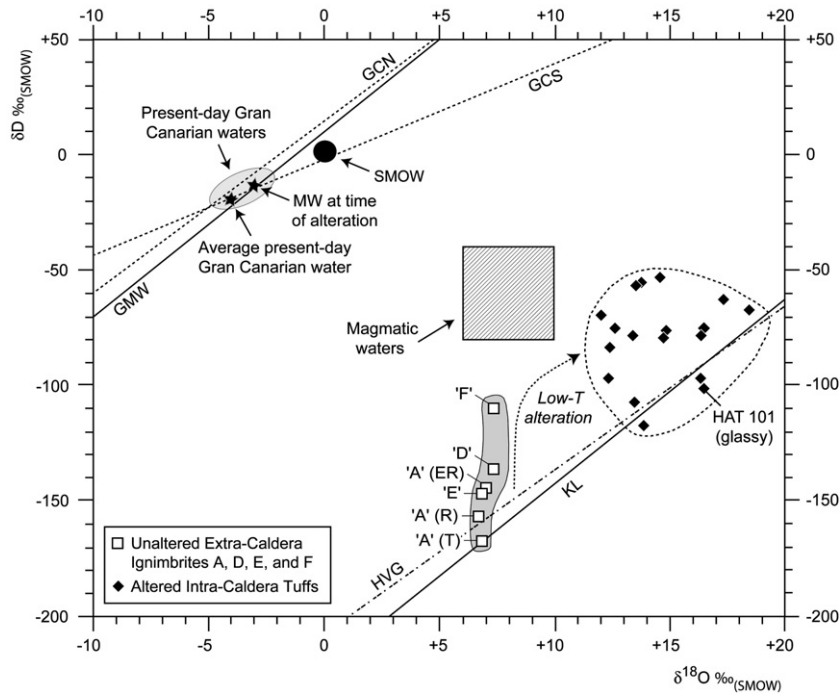


Fig. 9. Plot of whole-rock δD versus whole-rock $\delta^{18}O$ for the altered intra-caldera tuffs, and unaltered extra-caldera ignimbrites 'A' (ER = evolved rhyolite, R = rhyolite, T = trachyte), 'D', 'E' and 'F'. Also shown are the Global Meteoric Water Line (GMW) (Craig, 1961), the meteoric water lines for north (GCN) and south Gran Canaria (GCS) (Gonfiantini, 1973), the 'kaolinite' line (KL) (Savin and Epstein, 1970), and the 'hydrated volcanic glass' line (HVG) (Taylor, 1968). The fields for present-day Gran Canarian water (Javoy et al., 1986), Standard Mean Ocean Water (SMOW), and magmatic water (Taylor, 1986) are shown for reference, as well as the estimated composition of meteoric water at the time of alteration. Average δD and $\delta^{18}O$ values are plotted for samples analysed in duplicate. See Section 6.3 for details.

ignimbrite A (older) has the most negative δD values, while ignimbrite F (younger) has the least negative δD value (Fig. 8B). In addition, there is a systematic variation in δD within ignimbrite 'A' (a compositionally zoned ignimbrite), which displays the least depleted values at its base (evolved rhyolite; SiO_2 69–71 wt.%) and most depleted values at its top (trachyte; SiO_2 65–67 wt.%) (cf. Troll and Schmincke, 2002). This close coupling between δD and stratigraphic position/composition may in fact reflect differences in the extent of degassing between distinct, compositionally zoned Mogán magma chambers. On a plot of δD versus $\delta^{18}O$ (Fig. 9) the unaltered samples show no offset towards the 'kaolinite' line of Savin and Epstein (1970), or the 'hydrated volcanic glass' line of Taylor (1968), indicating that post-formational exchange with local precipitation ($\delta D = ca. -20\text{‰}$; $\delta^{18}O = ca. -4\text{‰}$; cf. Gonfiantini, 1973; Javoy et al., 1986) has not occurred. Thus, assuming the extra-caldera ignimbrites have not been affected by substantial alteration, these samples allow us to estimate the average H-isotope composition and water contents of the intra-caldera tuffs prior to hydrothermal activity (ca. -149‰ and 0.1 wt.%, respectively).

The δD of ambient meteoric water at the alteration site is estimated to have been ca. -15‰ , using the meteoric water line for southern Gran Canaria (Gonfiantini, in press) and a $\delta^{18}O$ of ca. -3‰ (see below). The altered intra-caldera tuffs have δD values ranging from -52‰ to -131‰ and H_2O concentrations up to ~ 4 wt.% (Fig. 8A, B). The distinct increase in both whole-rock δD values and water concentrations in the altered tuffs relative to unaltered ignimbrites can be explained by significant water–rock interaction. However, considering the equilibrium per mil H-isotope fractionation (ΔD) between most clay minerals and water is approximately -30‰ to -20‰ at 100–150 °C, and decreases in magnitude at higher temperatures (Sheppard and Gilg, 1996), it is unlikely that the clay-dominated assemblages of the altered tuffs ($\delta D_{\text{average}} = -84\text{‰}$) have equilibrated with ambient meteoric water with $\delta D = ca. -15\text{‰}$. Interaction of ambient meteoric water with pristine ignimbrites at low temperature (~ 100 – 150 °C)

would only account for whole-rock δD values of around -35‰ to -45‰ for the clay-rich altered tuffs. All altered tuff samples have δD values substantially lower than -45‰ , which might indicate interaction with a meteoric water source with a δD value significantly lower than -15‰ . At temperatures up to ~ 230 °C, there is a positive H-isotope fractionation between liquid water and water vapour (i.e. water vapour is depleted in D relative to the liquid water with which it is in equilibrium) (Horita and Wesolowski, 1994). Steam fumarole activity might, therefore, be a mechanism to produce water vapour with such low δD values in a hydrothermal environment. A modern analogue for this type of low-temperature system may be seen in e.g. New Zealand and Indonesia. Here, low-temperature steam fumaroles (~ 80 – 150 °C) are commonplace, and are known to fluctuate in intensity and isotopic composition due to environmental factors (e.g. Goff and Janik, 2000). Alternatively, it is possible that the range of whole-rock δD values for the altered tuffs reflect retrograde equilibration of clays and zeolites with present-day meteoric water ($\delta D = ca. -20\text{‰}$) at very low temperature (≤ 20 °C). However, Sheppard and Gilg (1996) suggest that clays are in fact rather robust minerals, in that they tend to record their original isotope composition at the time of formation, unless they have been subjected to more extreme conditions (e.g. a higher-temperature event). Thus, given the clay-rich nature of the altered tuffs, their whole-rock δD values should at least in part reflect interaction with an evolving, low- δD meteoric water source (such as steam fumaroles) during the Tejeda hydrothermal event, rather than post-formational exchange with present-day waters.

The $\delta^{18}O$ values of the altered samples from Fuente de Los Azulejos fall between 12 and 18‰ (Table 4; Fig. 9) and are up to 11.5‰ higher than those of the unaltered samples ($\delta^{18}O = 6.5$ – 7.1‰). The $\delta^{18}O$ values for the unaltered samples are within the typical range of igneous rocks (~ 6 – 8‰ ; Taylor, 1968), and are consistent with previous analyses of fresh igneous rocks on Gran Canaria (cf. Hansteen and Troll, 2003 and references therein). The $\delta^{18}O$ value of ambient meteoric water at the

alteration site has been estimated at ca. -3% , using the $\delta^{18}\text{O}$ -altitude correlation and meteoric water line for southern Gran Canaria (Gonfiantini, 1973), and an average recharge altitude of about 350–400 m above sea level (a.s.l.). The estimated altitude of recharge at the time of alteration is lower than at present (~ 600 to 700 m a.s.l.; cf. Javoy et al., 1986) as it takes into account an up to one-third increase in elevation (~ 300 – 350 m) caused by post-caldera cone-sheet emplacement (Schirnick et al., 1999), Plio-Quaternary igneous activity (Schmincke, 1982, 1998), and a fall in sea level of >100 m (Haq et al., 1987).

The secondary mineralogy of the altered tuffs (see Section 5.1) suggests that fluid temperatures were unlikely to have exceeded 200 – 250 °C at the sampling locality (cf. Deer et al., 1966; Thompson and Thompson, 1996). At 250 °C, $\Delta^{18}\text{O}_{\text{clay-water}}$ is approximately 5 – 7% (cf. Sheppard and Gilg, 1996). At lower temperatures, the magnitude of the clay–water oxygen fractionation increases, with $\Delta^{18}\text{O}_{\text{clay-water}}$ typically between 12 and 14% at 100 °C (cf. Sheppard and Gilg, 1996). Similarly, $\Delta^{18}\text{O}_{\text{zeolite-water}}$ is approximately 9% at 250 °C, and increases significantly at lower temperatures (cf. Chacko et al., 2001 and references therein). Thus, the relatively high $\delta^{18}\text{O}$ values of the altered tuffs most likely reflect clay and zeolite formation during low-temperature (≤ 250 °C) hydrothermal alteration, in which meteoric water ($\delta^{18}\text{O}_{\text{initial}} = \text{ca. } -3\%$) was the dominant fluid source. This is consistent with the findings of Cousens et al. (1992), who also invoked a meteoric water source for some less altered extra-caldera Mogán and Fataga tuffs. Furthermore, on a plot of $\delta^{18}\text{O}$ versus δD (Fig. 9), the altered tuffs show a clear offset towards the ‘kaolinite’ line of Savin and Epstein (1970), indicative of low-temperature, near-surface alteration and clay formation.

6.4. Numerical models

Numerical models were used to examine the stress field around an inflating magma chamber, in order to enhance our understanding of the structural controls on fluid flow that led to the intensity of hydrothermal alteration on Gran Canaria. Geothermal fluid migration in volcanic terrains is mainly controlled by tension fractures, which form (or are influenced by) the internal fluid pressure (Gudmundsson et al., 1997, 2002). Here, we examine the tensile stress for an inflating Gran Canaria magma chamber of Fataga age and depth.

For the stress models we used Poly3D, a three-dimensional boundary element code developed by the Stanford Rock Fracture Project (Thomas, 1993). The boundary element code is based on the analytical solutions for triangular dislocation sources in isotropic media (Comninou and Dundurs, 1975). We combined 400 triangular dislocations to a magma reservoir and placed it at the desired geometric location. At each element of the reservoir we defined traction boundary conditions. Traction allows simulating reservoir inflation by overpressure, which equals the total fluid pressure. The overpressure of magmatic bodies is generally between 5 and 40 MPa (Rubin, 1995). In our models, we simulated a magma overpressure of 10 MPa. We assigned a Poisson's ratio of $\nu=0.25$ and a Young's modulus of $E=70$ GPa.

The geometry and position of the Gran Canaria Fataga-age magma chamber is not precisely known, although some constraints are given by mineral thermobarometry (Schirnick, 1996), and structural studies of the Fataga-age cone sheets and extra-caldera ignimbrites (Schirnick et al., 1999). Based on these constraints, we simulated a sill-shaped Fataga magma chamber with a diameter of 10 km, emplaced at a depth of 3 – 5 km, and therefore a diameter/height aspect ratio of 5.0 . We calculated the tensile stress (σ_3) in a vertical cross-section through the center of the reservoir, ranging from the free surface to a depth of 10 km (Fig. 10).

Tensile stress during magma reservoir inflation is at a maximum (8 – 10 MPa) at the lateral edges of the sill-shaped reservoir (“d” in Fig. 10), and in a shallow zone extending from the surface to a depth of ~ 1 km directly above the inflating reservoir (“e” in Fig. 10). With increasing depth, the shallow, high-tensile stress zone divides into two zones (“f” in Fig. 10) of intermediate tensile stress (6 – 8 MPa) connected to the periphery of the magma chamber. Thus, for a recent caldera, tensile stress (and therefore fluid migration) may be dominant at a shallow level above the projected magma chamber. However, for a more deeply eroded caldera margin such as that associated with the Tejada caldera, fluid migration and near-surface hydrothermal alteration would be encouraged in the periphery of the projected magma reservoir. Directly above and below the reservoir (“g” in Fig. 10), tensile stress is low (<2 MPa), and fluid migration is expected to be of subordinate importance. The Fataga magma reservoir is thought to be somewhat larger in plan view than the typically associated outward-dipping ring fault structure seen at the surface (cf. Walter and Troll, 2001; Troll et al.,

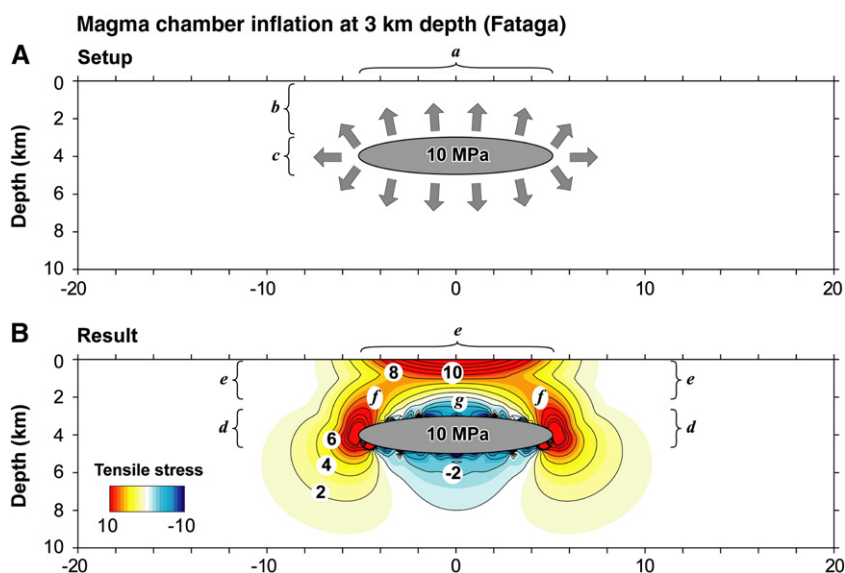


Fig. 10. (A,B): Numerical models of magma reservoir inflation. (A) Setup showing a cross-section through a shallow, Fataga-type magma reservoir. (B) Results showing the distribution of the maximum principal tensile stress. a – magma reservoir diameter: 10 km, b – distance from the top of the magma reservoir to the surface: 3 km, c – width of the reservoir: 2 km, d – periphery zone with increased tensile stress near the sides of the magma chamber, e – shallow zone of high tensile stress above the magma chamber, f – zone of intermediate tensile stress linking the deep periphery zone to the shallow central zone of maximum tensile stress, g – zone of low tensile stress directly above and below the magma reservoir.

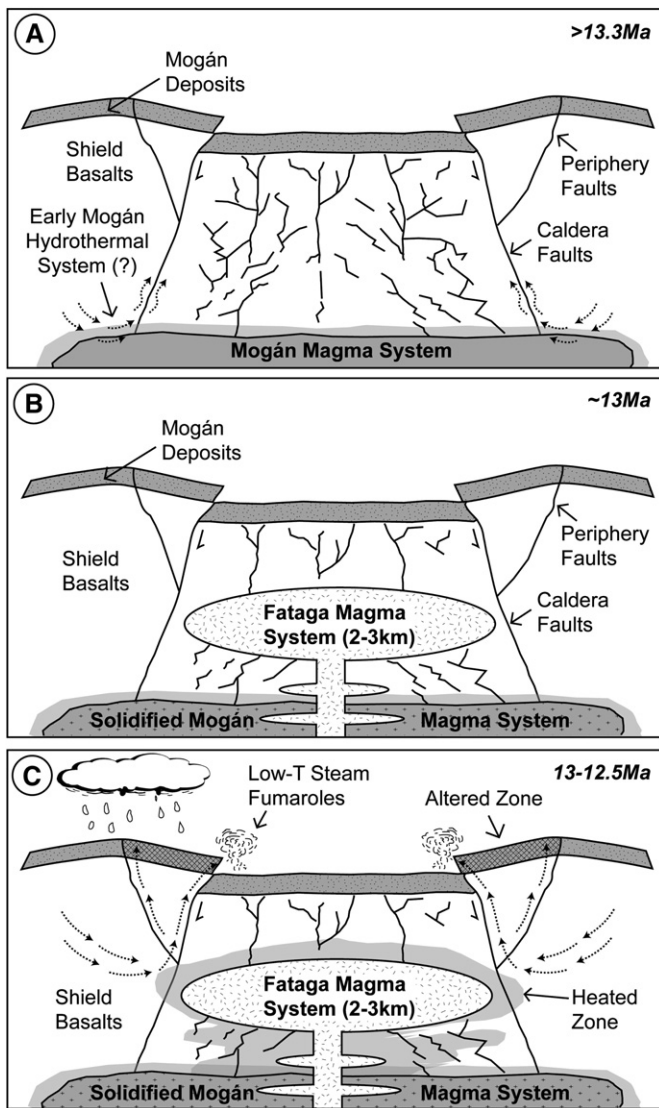


Fig. 11. (A–C): Cartoon sequence summarising evolution of Tejada hydrothermal system. (A) 14–13.3 Ma: collapse of the Tejada caldera along a steep, outward-dipping ring fault, accompanied by the eruption of the Mogán Group ignimbrites. Possible early Mogán hydrothermal upwelling associated with Mogán magma chamber emplacement and cooling. (B) 13 Ma: emplacement of the Fataga magma system ~2–3 km beneath Gran Canaria. (C) 13–12.5 Ma: formation of a heated zone around the Fataga magma system due to chamber emplacement and associated dyke intrusion. Elevated temperatures initiate radial inflow and upwelling of heated meteoric water and/or steam along the caldera periphery structures (e.g. faults and fracture systems). Dashed arrows show direction of fluid flow (cf. Taylor and Forester, 1970; Larson and Taylor, 1986). The hydrothermal fluids are discharged at the surface, perhaps in the form of low-temperature steam fumaroles, resulting in pervasive alteration of Mogán/Fataga transitional stage ignimbrites.

2002). We therefore expect hydrothermal flow to be best developed in a zone that extends from the main caldera fault system (located within the Tejada caldera; cf. Troll et al., 2002 and references therein) to the caldera periphery. Our numerical modeling result is therefore in accordance with our observations from Gran Canaria, and supports the hypothesis that shallow magma chamber emplacement and associated inflation caused preferential alteration around shallow-level caldera periphery structures.

6.5. Constraints on the Tejada hydrothermal event

The intra-caldera and extra-caldera faults and fractures of the Tejada caldera system are thought to have extended from the surface

to the Mogán magma chamber (Schmincke, 1998; Troll et al., 2002). These faults would have provided pathways for fluid entry and subsequent hydrothermal circulation.

The proposed timing of hydrothermal alteration at Fuente de Los Azulejos coincides with the emplacement of the Fataga magma system at a shallow level (2–3 km) below Gran Canaria (Schirnack, 1996; Bogaard and Schmincke, 1998; Schmincke, 1998; Schirnack et al., 1999). Our numerical modeling results support the hypothesis that this shallow magma chamber emplacement and inflation provided the heat source and pathways for hydrothermal circulation and alteration at shallow-level caldera periphery structures. Controversy exists, however, in respect to the exact timing and spatial extent of the hydrothermal activity on Gran Canaria. Pérez Torrado et al. (2004) and Cabrera Santana et al. (2006) describe mid-Mogán rocks that are more strongly altered to the northwest of our sample site, suggesting that hydrothermal activity may have persisted throughout Mogán time (perhaps in pulses), and reached its maximum spatial extent at the Mogán/Fataga transition. Alternatively, the rocks lower in the stratigraphy (and so closer to the heat source) could have been more strongly altered solely during Fataga magma chamber emplacement (cf. Schmincke, 1998).

Our sample set is derived from the topmost alteration horizon of late Mogán/early Fataga age, and is therefore insufficient to address this problem in full. However, our samples do allow us to characterise the final and/or maximum spatial extent of the hydrothermal system. Establishment of the Fataga magma chamber system at a shallow level was accompanied by frequent dyke intrusion into the intra-caldera zone, and probably also the caldera ring fault zone (Schmincke, 1998; Schirnack et al., 1999). Elevated temperatures resulting from chamber and dyke emplacement may have led to boiling of meteoric water and loss of fluid as vapour. At temperatures up to ~230 °C, water vapour is depleted in D relative to the water with which it is in equilibrium (Horita and Wesolowski, 1994). Such D-depleted water vapour would have ascended from the area of formation near the magma chamber, via fractures and faults in the caldera periphery and via porous flow through the intra-caldera tuffs, creating a zone of hydrothermal upwelling between the surface and the intrusion site (cf. Taylor and Forester, 1970; Larson and Taylor, 1986). The water vapour would have eventually exited at the surface, perhaps in the form of low-temperature steam fumaroles. Prolonged interaction with steam at the surface would have resulted in altered rocks with more negative δD values than rocks that had simply interacted with ambient meteoric water. Although it is difficult to assess the precise processes of H-isotope fractionation, and a combination of processes may have been at work, alteration by water vapour offers a very effective mechanism to produce the lower than expected δD values of the altered tuffs.

Overall, the results from the intra-caldera tuffs on Gran Canaria are consistent with low-temperature alteration in the shallow, epithermal part of a larger, fault-controlled hydrothermal system associated with emplacement of the high-level Fataga magma chamber system (Fig. 11A–C). Water and/or steam would have migrated along caldera periphery structures, and through the intra-caldera tuffs via porous flow. The main source of water was meteoric, and fluid temperatures most likely did not exceed ~200–250 °C in the near-surface environment. This suggests that modern analogues to the Tejada hydrothermal system may be seen in presently active volcanic areas such as New Zealand and Indonesia (e.g. Hochstein and Browne, 2000; Goff and Janik, 2000). The phenomena on Gran Canaria can therefore be used as a dissected analogue for the architecture of active hydrothermal systems that are inaccessible at present.

Acknowledgements

Robbie Goodhue (XRD), Dagmar Rau (XRF), and Fayrooza Rawoot (stable isotopes) are thanked for their help during data acquisition.

Assistance in the field from Alejandro Rodríguez González is greatly appreciated. Special thanks to Hans-Ulrich Schmincke for discussion and advice. George Sevastopulo, John Gamble, Mari Sumita, Thor Hansteen, Chris Stillman, and John Wolff are thanked for additional fruitful discussions throughout our study. The manuscript was improved by the helpful reviews of Juan Carlos Carracedo and Peter Larson. Financial support from the Irish Research Council for Science, Engineering, and Technology (IRCSET), and from Trinity College Dublin, is greatly appreciated.

References

- Abratis, M., Schmincke, H.-U., Hansteen, T.H., 2002. Composition and evolution of submarine volcanic rocks from the central and western Canary Islands. *International Journal of Earth Sciences* 91, 562–582.
- Bogaard, P., Schmincke, H.-U., 1998. Chronostratigraphy of Gran Canaria. In: Weaver, P.P.E., Schmincke, H.-U., Firth, J.V., Duffield, W. (Eds.), *Proceedings of the Ocean Drilling Program. Scientific Results*, vol. 157, pp. 127–140.
- Borthwick, J., Harmon, R.S., 1982. A note regarding ClF_3 as an alternative to BrF_5 for oxygen isotope analysis. *Geochimica et Cosmochimica Acta* 46, 1665–1668.
- Cabrera Santana, M.C., Pérez Torrado, F.J., Antón Gil, A., Muñoz Sanz, F., 2006. Volcanología de los Azulejos y su relación con las aguas subterráneas del Valle de La Aldea (Gran Canaria). Cabildo de Gran Canaria, Las Palmas de Gran Canaria, pp. 1–153.
- Chacko, T., Cole, D.R., Horita, J., 2001. Equilibrium oxygen, hydrogen and carbon isotope fractionation factors applicable to geologic systems. In: Valley, J.W., Cole, D.R. (Eds.), *Stable Isotope Geochemistry. Reviews in Mineralogy and Geochemistry*, vol. 43, pp. 1–82.
- Comninou, M., Dundurs, J., 1975. Angular dislocation in a half space. *Journal of Elasticity* 5, 203–216.
- Coplen, T.B., 1995. Reporting of stable hydrogen, carbon, and oxygen isotopic abundances. *Geothermics* 24, 707–712.
- Coplen, T.B., Kendall, C., Hoppie, J., 1983. Comparison of stable isotope reference samples. *Nature* 302, 236–238.
- Cousens, B.L., Spera, F.J., Tilton, G.R., 1990. Isotopic patterns in silicic ignimbrites and lava flows of the Mogán and lower Fataga formations, Gran Canaria, Canary Islands: temporal changes in mantle source compositions. *Earth and Planetary Science Letters* 96, 319–335.
- Cousens, B.L., Spera, F.J., Dobson, P.F., 1992. Post-eruptive alteration of silicic ignimbrites and lavas, Gran Canaria, Canary Islands: strontium, neodymium, lead and oxygen isotopic evidence. *Geochimica et Cosmochimica Acta* 57, 631–640.
- Craig, H., 1961. Isotopic variations in meteoric waters. *Science* 133, 1702–1703.
- Deer, W.A., Howie, R.A., Zussman, J., 1966. *An Introduction to the Rock-Forming Minerals*. Longman Scientific and Technical, Essex, pp. 1–528.
- Freundt, A., Schmincke, H.-U., 1995. Petrogenesis of rhyolite–trachyte–basalt composite ignimbrite P1, Gran Canaria, Canary Islands. *Journal of Geophysical Research* 100, 455–474.
- García del Cura, M.A., La Iglesia, A., Ordóñez, S., 1999. Zeolitas (clinoptilolita-analcima-filipsita) en depósitos piroclásticos miocenos del borde de la caldera de Tejeda (Gran Canaria, Islas Canarias). *Revista de la Sociedad de España* 12, 229–241.
- Gerbe, M.C., Thouret, J.C., 2004. Role of magma mixing in the petrogenesis of tephra erupted during the 1990–98 explosive activity of Navado Sabancaya, southern Peru. *Bulletin of Volcanology* 66, 541–561.
- Goff, F., Janik, C.J., 2000. Geothermal systems. In: Sigurdsson, H., Houghton, B.F., McNutt, S.R., Rymer, H., Stix, J. (Eds.), *Encyclopedia of Volcanoes*. Academic Press, California, pp. 817–834.
- Gonfiantini, R., 1973. Isotope study of Canary Islands groundwater. Internal Report, Project SPA/69/515, International Atomic Energy Agency (isotope hydrology section), Vienna, Austria, pp. 1–21.
- Gudmundsson, A., Marti, J., Turon, E., 1997. Stress fields generating ring faults in volcanoes. *Geophysical Research Letters* 24, 1559–1562.
- Gudmundsson, A., Fjeldskaar, I., Brenner, S.L., 2002. Propagation pathways and fluid transport of hydrofractures in jointed and layered rocks in geothermal fields. *Journal of Volcanology and Geothermal Research* 116, 257–278.
- Hansteen, T.H., Troll, V.R., 2003. Oxygen isotope composition of xenoliths from the oceanic crust and volcanic edifice beneath Gran Canaria (Canary Islands): consequences for crustal contamination of ascending magmas. *Chemical Geology* 193, 181–193.
- Harris, C., Erlank, A.J., 1992. The production of large-volume low- $\delta^{18}\text{O}$ rhyolites during the rifting of Africa and Antarctica: the Lebombo monocline, southern Africa. *Geochimica et Cosmochimica Acta* 56, 3561–3570.
- Haq, B.U., Hardenbol, J., Vail, P.R., 1987. Chronology of fluctuating sea levels since the Triassic. *Science* 235, 1156–1167.
- Hill, I.G., Worden, R.H., Meighan, I.G., 2001. Formation of interbasaltic laterite horizons in NE Ireland by early Tertiary weathering processes. *Proceedings of the Geologists Association* 112, 339–348.
- Hochstein, M.P., Browne, P.R.L., 2000. Surface manifestations of geothermal systems with volcanic heat sources. In: Sigurdsson, H., Houghton, B.F., McNutt, S.R., Rymer, H., Stix, J. (Eds.), *Encyclopedia of Volcanoes*. Academic Press, California, pp. 835–855.
- Horita, J., Wesolowski, D.J., 1994. Liquid–vapor fractionation of oxygen and hydrogen isotopes of water from the freezing to the critical temperature. *Geochimica et Cosmochimica Acta* 58, 3425–3437.
- Javoy, M., Stillman, C.J., Pineau, F., 1986. Oxygen and hydrogen isotope studies on the basal complexes of the Canary Islands: implications on the conditions of their genesis. *Contributions to Mineralogy and Petrology* 92, 225–235.
- Kobberger, G., Schmincke, H.-U., 1999. Deposition of rheomorphic ignimbrite D (Mogán Formation), Gran Canaria, Canary Islands, Spain. *Bulletin of Volcanology* 60, 465–485.
- Larson, P.B., Taylor Jr., H.P., 1986. An oxygen isotope study of hydrothermal alteration in the Lake City Caldera, San Juan Mountains, Colorado. *Journal of Volcanology and Geothermal Research* 30, 47–82.
- Le Maitre, R.W., Bateman, O., Dudek, A., Keller, J., Lameyre Le Bas, M.J., Sabine, P.A., Schmid, R., Sorensen, H., Streckeisen, A., Woolley, A.R., Zanettin, B., 1989. *A Classification of Igneous Rocks and Glossary of Terms*. Blackwell, Oxford, pp. 1–206.
- Nabelek, P.I., O’Neil, J.R., Papike, J.J., 1983. Vapour phase exsolution as a controlling factor in hydrogen isotope variation in granitic rocks: the Notch Peak granitic stock, Utah. *Earth and Planetary Science Letters* 66, 137–150.
- Pérez Torrado, F.J., Cabrera Santana, M.C., Antón Gil, A., Muñoz Sanz, F., 2004. Estratigrafía y petrología de los depósitos de “Azulejos” del borde de la Caldera de Tejeda (Gran Canaria, Islas Canarias). *Geotemas* 6, 159–162.
- Rubin, A.N., 1995. Getting granite dykes out of the source region. *Journal of Geophysical Research-Solid Earth* 100, 5911–5929.
- Savin, S.M., Epstein, S., 1970. Oxygen and hydrogen isotope geochemistry of clay minerals. *Geochimica et Cosmochimica Acta* 34, 25–42.
- Schirnick, C., 1996. Formation of an intracaldera cone sheet dike swarm (Tejeda caldera, Gran Canaria). PhD thesis, Christian-Albrechts-Universität, Kiel, Germany.
- Schirnick, C., van den Bogaard, P., Schmincke, H.-U., 1999. Cone sheet formation and intrusive growth of an oceanic island – the Miocene Tejeda Complex on Gran Canaria (Canary Islands). *Geology* 27, 207–210.
- Schmincke, H.-U., 1969. *Petrologie der phonolithischen bis rhyolithischen Vulkanite auf Gran Canaria*. Kanarische Inseln. PhD thesis, Universität Heidelberg, Germany.
- Schmincke, H.-U., 1976. The geology of the Canary Islands. In: Kunkel, G. (Ed.), *Biogeography and Ecology in the Canary Islands*. W. Junk, The Hague, pp. 67–184.
- Schmincke, H.-U., 1982. Volcanic and chemical evolution of the Canary Islands. In: von Rad, U., Hinz, K., Sarnthein, M., Seibold, E. (Eds.), *Geology of the Northwest African Continental Margin*. Springer-Verlag, Berlin, pp. 273–306.
- Schmincke, H.-U., 1998. *Geological Field Guide of Gran Canaria (Part 1 and 2)*. Pluto Press, Witten, pp. 1–64.
- Schmincke, H.-U., Swanson, D.A., 1966. Eine alte caldera auf Gran Canaria. *Neues Jahrbuch für Geologische und Paläontologische Mitteilungen* 5, 260–269.
- Schröcke, H., Weiner, K.-L., 1981. *Mineralogie*. De Gruyter Publications, The Netherlands, pp. 1–952.
- Sheppard, S.M.F., Gilg, H.A., 1996. Stable isotope geochemistry of clay minerals: the story of sloppy, sticky, lumpy and tough. *Clay Minerals* 31, 1–24.
- Shevenell, L., Goff, F., 1995. The use of tritium in groundwater to determine fluid mean residence times of Valles caldera hydrothermal fluids. *Journal of Volcanology and Geothermal Research* 67, 187–205.
- Sumita, M., Schmincke, H.-U., 1998. Tephra event stratigraphy and emplacement of volcanoclastic sediments, Mogán and Fataga stratigraphic intervals, Part 1: mineral and chemical stratigraphy of volcanoclastic units and correlation to the subaerial record. In: Weaver, P.P.E., Schmincke, H.-U., Firth, J.V., Duffield, W. (Eds.), *Proceedings of the Ocean Drilling Program. Scientific Results*, vol. 157, pp. 219–264.
- Taylor, B.E., 1986. Magmatic volatiles: isotopic variation of C, H, and S. In: Valley, J.W., Taylor Jr., H.P., O’Neil, J.R. (Eds.), *Stable Isotopes in High Temperature Geological Processes. Reviews in Mineralogy*, vol. 16, pp. 185–225.
- Taylor Jr., H.P., 1968. The oxygen isotope geochemistry of igneous rocks. *Contributions to Mineralogy and Petrology* 19, 1–71.
- Taylor Jr., H.P., Forester, R.W., 1970. Low $\delta^{18}\text{O}$ igneous rocks from the intrusive complexes of Skye, Mull, and Ardnamurchan, western Scotland. *Journal of Petrology* 12, 465–497.
- Taylor, B.E., Eichelberger, J.C., Westrich, H.R., 1983. Hydrogen isotopic evidence of rhyolitic magma degassing during shallow intrusion and eruption. *Nature* 306, 541–545.
- Thomas, A.L., 1993. Poly3D: a three dimensional, polygonal element, displacement discontinuity boundary element computer program. M.S. thesis, Stanford University, Stanford, CA, USA.
- Thompson, A.J.B., Thompson, J.F.H. (Eds.), 1996. *Atlas of Alteration: a Field and Petrological Guide to Hydrothermal Alteration Minerals*. Alpine Press Limited, Vancouver, pp. 1–119.
- Troll, V.R., 2001. Evolution of large peralkaline silicic magma chambers and associated caldera systems: a case study from Gran Canaria, Canary Islands. PhD thesis, Christian-Albrechts-Universität, Kiel, Germany.
- Troll, V.R., Schmincke, H.-U., 2002. Alkali-feldspar in compositionally zoned peralkaline rhyolite/trachyte ignimbrite “A”, Gran Canaria: implications for magma mixing and crustal recycling. *Journal of Petrology* 43, 243–270.
- Troll, V.R., Walter, T.R., Schmincke, H.-U., 2002. Cyclic caldera collapse: piston or piecemeal subsidence? Field and experimental evidence. *Geology* 30, 135–138.
- Troll, V.R., Sachs, P.M., Schmincke, H.-U., Sumita, M., 2003. The REE–Ti mineral chevkinite in comenditic magmas from Gran Canaria, Spain: a SYXRF-probe study. *Contributions to Mineralogy and Petrology* 145, 730–741.
- Varnes, D., 1963. *Geology and ore deposits of the South Silverton mining area, San Juan County, Colorado*. U.S. Geological Survey Professional Paper 378-A, 1–56.
- Vennemann, T.W., Smith, H.S., 1990. The rate and temperature of reaction of ClF_3 with silicate minerals, and their relevance to oxygen isotope analysis. *Chemical Geology* 86, 83–88.
- Vennemann, T.W., O’Neil, J.R., 1993. A simple and inexpensive method of hydrogen isotope and water analyses of minerals and rocks based on zinc reagent. *Chemical Geology* 103, 227–234.
- Walter, T.R., Troll, V.R., 2001. Formation of caldera periphery faults: an experimental study. *Bulletin of Volcanology* 63, 191–203.